Supporting information

A novel anode for direct borohydride-hydrogen peroxide fuel cell: Au nanoparticles decorated 3D self-supported reduced graphene oxide foam

Biaopeng Li, Congying Song, Xiaomei Huang*, Ke Ye, Kui Cheng, Kai Zhu, Jun Yan, Dianxue Cao, Guiling Wang*

Key Laboratory of Superlight Materials and Surface Technology of Ministry of Education, College of Materials Science and Chemical Engineering. Harbin Engineering University, Harbin, 150001, P.R.China.

Corresponding Authors：

Guiling Wang* E-mail: wangguiling@hrbeu.edu.cn

Xiaomei Huang* E-mail: huangxiaomei@hrbeu.edu.cn

Table of Contents

Flexibility display of rGO foam and Au-NP@eGO foam electrode

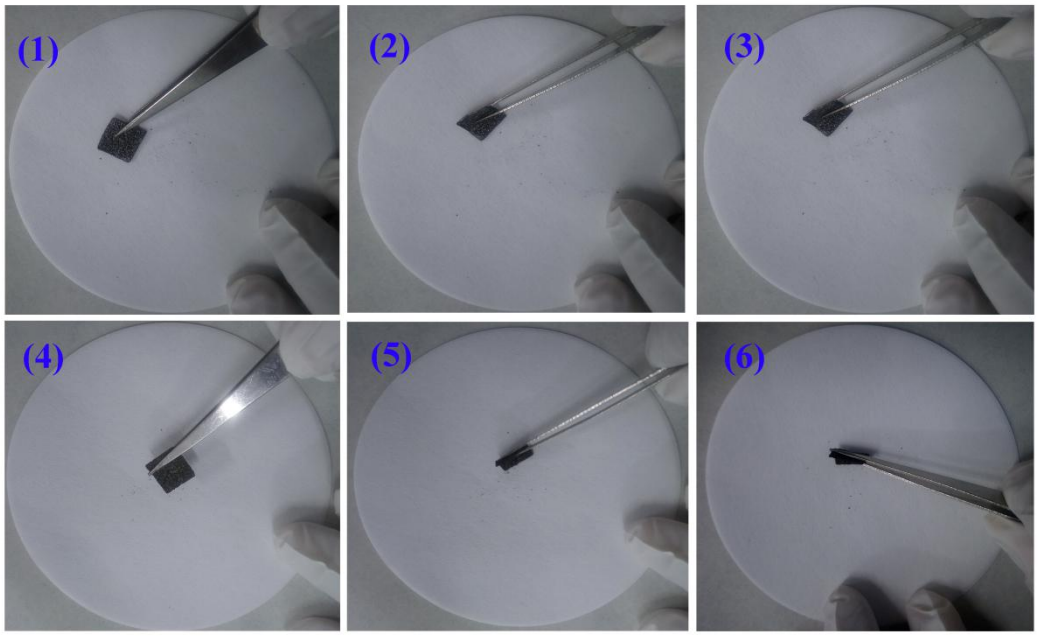

Fig. S1 The flexibility display of rGO foam.

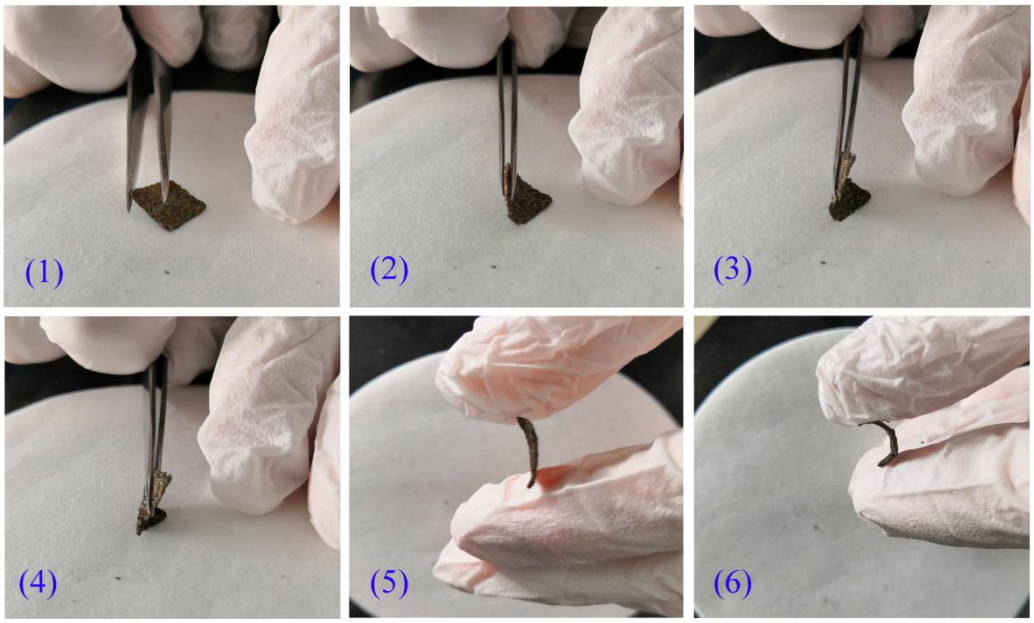

Fig. S2 The flexibility display of Au-NP@rGO foam electrode.

SEM images of Au-NP@Ni foam electrode

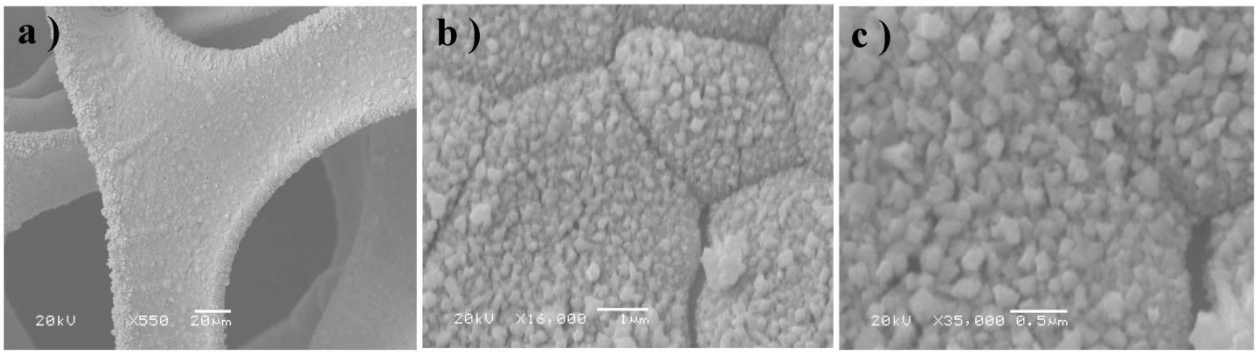

Fig. S3 SEM images of Au-NP@Ni foam electrode.

The electrochemical active surface area of Au-NP@Ni foam electrode

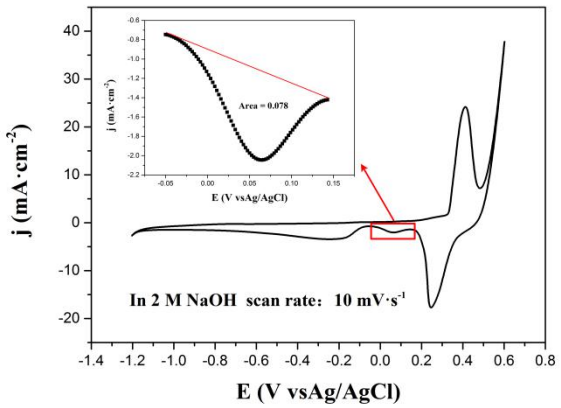

Fig. S4 A wide potential window CV tests of Au-NP@Ni foam electrode that tested in 2 mol·L^{-1} NaOH at a scan rate of 10 mV·s^{-1}.

Study on kinetic parameters in NaBH4 oxidation reaction

The oxidation of $NaBH_4$ on the Au-NP@rGO foam and Au-NP@Ni foam electrode can be evaluated by the following equation [S1]:

$$j_p = zC_{NaBH_4}^{\beta} \qquad (Eq.\ S1)$$

Where j_p is the peak current density ($A \cdot cm^{-2}$), z is a constant, C refers to the $NaBH_4$ concentration ($mol \cdot cm^{-3}$) and β is the reaction order concerning C_{NaBH_4}. According to the slopes of $ln\ j$ vs. $ln\ C_{NaBH_4}$ plots in Fig. 4(c) and Fig. S5(c), the value of β is calculated as 0.96 and 0.95 on Au-NP@rGO foam and Au-NP@Ni foam electrode, respectively.

The relationship between peak potential, E_p (V), and scan rate ν ($V \cdot s^{-1}$) for an irreversible electrochemical process can be described by Eq. S2 [S2].

$$E_p = E^0 + \left[\frac{RT}{(1-\alpha)n_a F}\right]\left\{0.78 + \ln\frac{D}{k_s} + \ln\left[\frac{(1-\alpha)n_a F\nu}{RT}\right]^{1/2}\right\} \qquad (Eq.\ S2)$$

where E^0 is the formal potential (V), R is the universal gas constant (8.314 $JK^{-1} \cdot mol^{-1}$), T is the temperature (K), α is the charge transfer coefficient, n_a is the number of electrons involved in the rate-determining step, F is the Faraday constant (96485 $C \cdot mol^{-1}$), D is the diffusion coefficient of BH_4^- ($cm^2 \cdot s^{-1}$) and k_s is the standard heterogeneous rate constant ($cm \cdot s^{-1}$).

$D_{BH_4^-}$ values at different temperatures used for evaluation of n, were calculated

using the expression proposed by Wang and coworkers [S3] (Eq. (S3)) that takes into account $D_{BH_4^-}$ change with the temperature, which is valid for 2 M NaOH solutions and does not depend on BH_4^- concentration.

$$D_{BH_4^-} = 5.57 \times 10^{-3} \exp\left(\frac{-15.2 \times 10^3}{RT}\right) \qquad (Eq.\ S3)$$

The values calculated from Eq. (S3) were multiplied by 2, as recent precise $D_{BH_4^-}$ determination [S4] has shown that exact $D_{BH_4^-}$ values are twice of those generally reported in the literature.

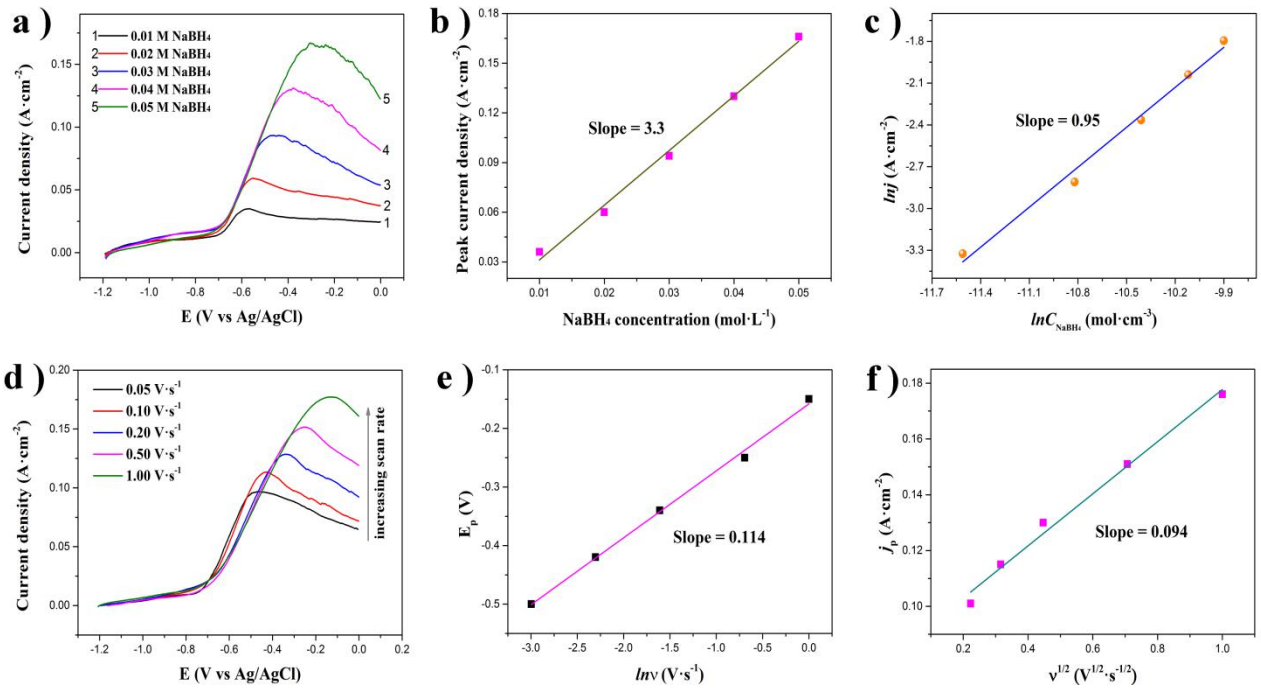

Fig. S5 LSV curves of Au-NP@Ni foam electrode under different concentration of $NaBH_4$ and 2 M NaOH at a scan rate of 50 $mV \cdot s^{-1}$ (a) and the corresponding j_p vs. C_{NaBH4} plots (b), lnj_p vs. lnC_{NaBH4} plots (c). LSV curves recorded at different ν of Au-NP@Ni foam electrode in 2 M NaOH and 0.03M $NaBH_4$ (d) with the dependence of E_p on ln ν (e) and dependence of j_p on $\nu^{1/2}$ (f).

Utilization of $NaBH_4$ on Au-NP@rGO foam electrode

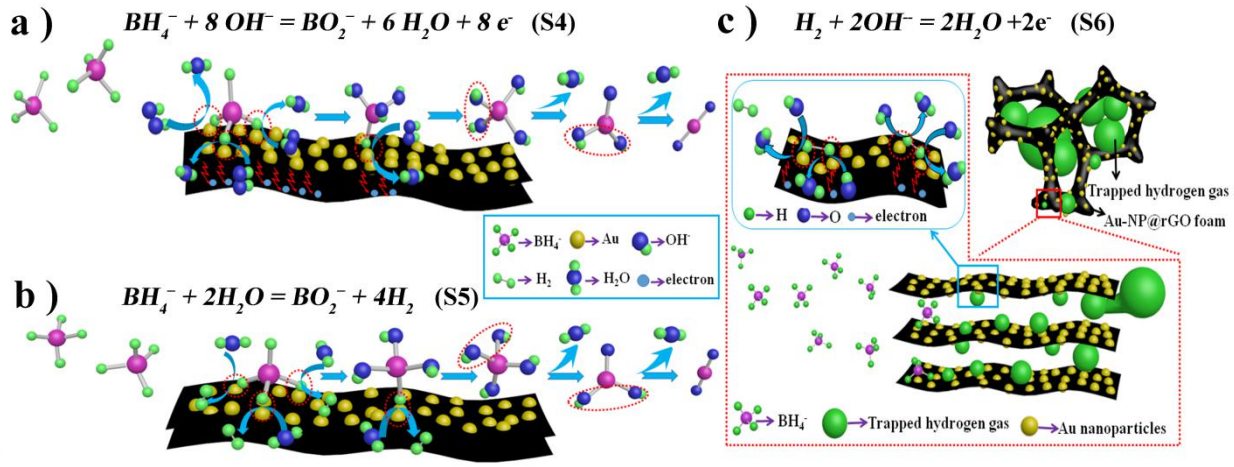

Fig. S6 Schematic diagram of electro-oxidation of $NaBH_4$ (a), hydrolysis of $NaBH_4$ (b) and the electro-oxidation of trapped hydrogen which produced by the hydrolysis of $NaBH_4$ (c).

Electrochemical impedance study

Fig. S7(a) shows the Nyquist plots under the situations of absence and presence of $NaBH_4$ at -0.1 V. Without $NaBH_4$, the Nyquist plots contain a semicircle in the high-frequency region and a straight line in the low-frequency region which indicates that electrochemical process is controlled by both charge transfer process and diffusion processes. When $NaBH_4$ was added to the solution, the Nyquist plots displayed two adjacent semicircles in high and low-frequency regions, respectively. From the comparison of Nyquist plots in Fig. S7(a), it is not difficult to conclude that when $NaBH_4$ is added to the solution, the semicircles in low-frequency regions can be attributed to the direct oxidation of $NaBH_4$. Besides, the Nyquist plots in 2 $mol \cdot L^{-1}$ NaOH and 0.4 $mol \cdot L^{-1}$ $NaBH_4$ at different potentials

were displayed in Fig. S7(b). With the polarization potential moving to a more positive value, the charge transfer resistance displayed an unceasingly decreased trend. This phenomenon implies that a more positive potential is beneficial to reduce the charge transfer resistance and accelerate the electrooxidation of $NaBH_4$ [S5].

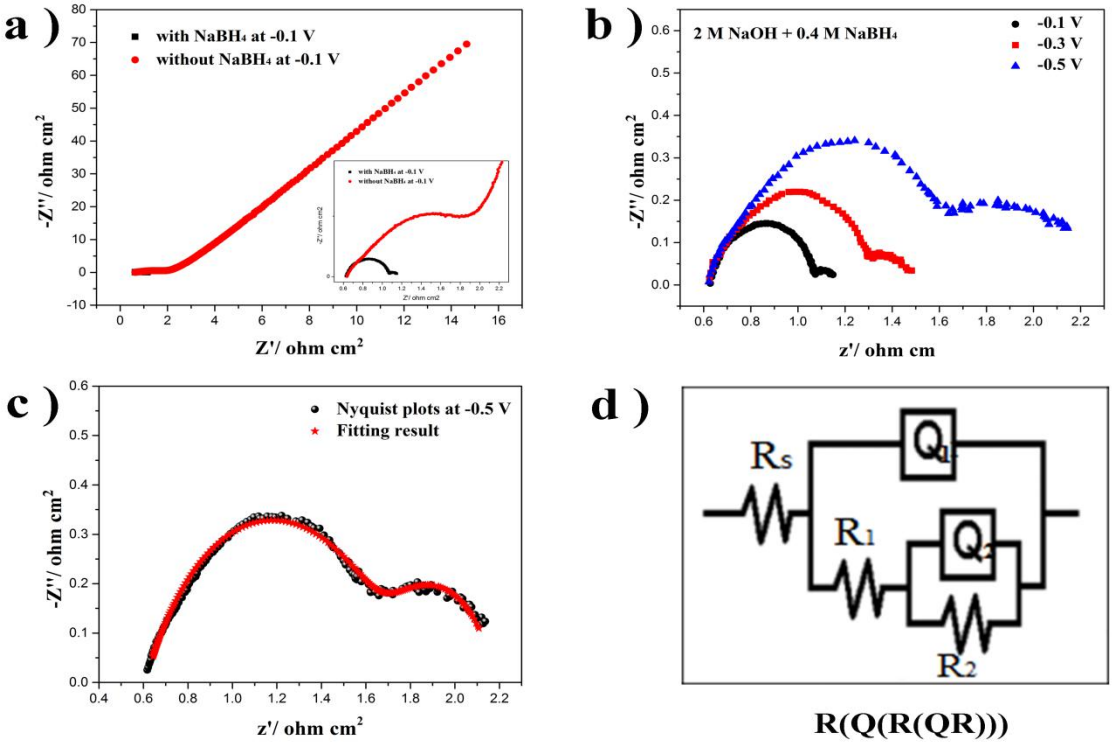

Fig. S7 Nyquist plots in the situations of presence and absence of $NaBH_4$ at -0.1 V (a). Nyquist plots at different potentials in 2 mol·L^{-1} NaOH and 0.4 mol·L^{-1} $NaBH_4$ (b). Nyquist fitting curves (c) and the corresponding equivalent circuit diagrams (d).Frequency range:100 kHz to 10 mHz.

The Nyquist fitting curve was shown in Fig. S7(c), and ZSimDemo software was used to perform the fitting. Fig. S7(d) shows the corresponding equivalent circuit diagram. In the equivalent circuit diagram, R_s is the solution resistance; R_1 means the charge transfer resistance of the transition between Au oxide and Au [S6];

R_2 represents the charge transfer resistance of direct electrooxidation of $NaBH_4$ on the electrode. Q_1 and Q_2 are the constant phase element (CPE). The specific value of each component is shown in Table. S1. The value of solution resistance (R_s) of Au-NP@rGO foam electrode in 2 M NaOH and 0.4 M $NaBH_4$ is 0.6 Ω, which reveals the good conductivity of the electrode in the test solution. When the positive move the potential from -0.5 V to -0.1 V, the charge transfer resistance (R_1) of the transition between Au oxide and Au is reduced from 1.133 to 0.447 Ω, indicating that a more positive potential is helpful for the regeneration of the Au catalyst. Also, with the positive move of potential, charge transfer resistance of direct electrooxidation of $NaBH_4$ (R_2) is decreased from 0.397 to 0.108 Ω reveals that the oxidation of $NaBH_4$ is easier to occur at a positive potential. The minimal charge transfer resistance of $NaBH_4$ electrooxidation reaction implies that Au-NP@rGO foam electrode is a high-efficiency catalyst.

Table. S1 The value of each circuit component at different potentials

Potential (V)	Rs ($\Omega \cdot cm^2$)	Q_1-Yo ($\Omega^{-1} \cdot m^{-2} \cdot s^n$)	Q_1-n	R_1 ($\Omega \cdot cm^2$)	Q2-Yo ($\Omega^{-1} \cdot m^{-2} \cdot s^n$)	Q_2-n	R_2 ($\Omega \cdot cm^2$)
-0.5	0.61	0.003056	0.7693	1.133	0.1112	0.7528	0.397
-0.3	0.60	0.002918	0.7693	0.764	0.8056	0.7852	0.231
-0.1	0.62	0.000872	0.8603	0.447	0.8781	0.6795	0.108

Fuel cell performance comparison

Table S2. Fuel cell Performance Comparison for Various Reported Anode

Anode catalyst	Cathode catalyst	Anode fuel	Cathodic oxidant	Open-circle voltage (V)	Power density ($mW \cdot cm^{-2}$)	ref
Au/C (0.17 mg Au cm^{-2})	Pt mesh	0.5 M $NaBH_4$ +2 M NaOH	4.5 M H_2O_2 + 2.0 M HCl	1.41	8.72	[S5]
$Au_2Ni_1Cu_1$/C (0.17 mg metal cm^{-2})	Pt mesh	0.5 M $NaBH_4$ +2 M NaOH	4.5 M H_2O_2 + 2.0 M HCl	1.78	60.51	[S5]
Au/C (2 mg of Au cm^{-2})	Pt/C	2.5 M NaOH + 1.32 M $NaBH_4$	O_2	-	72	[S7]
Pt/PPy-$C_{35\%}$ (0.05 mg of Pt cm^{-2})	Pt/PPy-$C_{35\%}$	1 M $NaBH_4$ + 4 M NaOH	5 M H_2O_2 + 1.5 M HCl	1.77	59.6	[S8]
Pt/C (4 mg of Pt cm^{-2})	Pt/C	3 M NaOH + 1 M $NaBH_4$	2 M H_2O_2 + 0.5 M H_2SO_4	1.66	35	[S9]
Pt/C	Pt mesh	2 M NaOH + 0.5 M $NaBH_4$	4.5 M H_2O_2 + 2.0 M HCl	1.8	31.4	[S10]
Pd(hollow)/C (0.9 mg of Pd cm^{-2})	Pt/C	3 M NaOH + 1 M $NaBH_4$	2 M H_2O_2 + 1 M H_2SO_4	1.84	48.4	[S10]
Au/C (0.9 mg metal cm^{-2})	Au/C	1 M $NaBH_4$ + 3 M NaOH	2 M H_2O_2 + 0.5 M H_2SO_4	1.6	21.8	[S11]
$Au_{50}Fe_{50}$/C (0.9 mg metal cm^{-2})	Au/C	1 M $NaBH_4$ + 3 M NaOH	2 M H_2O_2 + 0.5 M H_2SO_4	1.6	34.9	[S11]
Au@CoB (70 mg cm^{-2})	$LaNi_{0.9}Ru_{0.1}O_3$/ CNT/Ni foam	0.8 M KBH_4 + 6 M KOH	Air	1.07	85	[S12]
pure Au	$LaNi_{0.9}Ru_{0.1}O_3$/ CNT/Ni foam	0.8 M KBH_4 + 6 M KOH	Air	1	46	[S12]
Pt/C pasted on carbon cloth ($0.5mg \cdot cm^{-2}$)	commercial Pt/C	1 M $NaBH_4$ + 5 M NaOH	pure oxygen	0.92	46.5	[S13]
Au-NP@rGO foam (1.7 mg metal cm^{-2})	Pd/C	0.4 M $NaBH_4$ + 2 M NaOH	2 M H_2O_2 + 0.8 M H_2SO_4	1.63	60	This work

Reference

[S1]Šljukić, B.; Milikić, J.; Santos, D. M. F.; Sequeira, C. A. C.; Macciò, D.; Saccone, A. Electrocatalytic performance of Pt–Dy alloys for direct borohydride fuel cells. J. Power Sources 2014, 272, 335-343, DOI: 10.1016/j.jpowsour.2014.08.080.

[S2]Santos, D. M. F.; Sequeira, C. A. C. Cyclic voltammetry investigation of borohydride oxidation at a gold electrode. Electrochim. Acta 2010, 55 (22), 6775-6781, DOI: 10.1016/j.electacta.2010.05.091.

[S3]Wang, K.; Lu, J.; Zhuang, L. Direct determination of diffusion coefficient for borohydride anions in alkaline solutions using chronoamperometry with spherical Au electrodes. J. Electroanal. Chem. 2005, 585 (2), 191-196, DOI: 10.1016/j.jelechem.2005.08.009.

[S4]Chatenet, M.; Lima, F. H. B.; Ticianelli, E. A. Gold is not a Faradaic-Efficient Borohydride Oxidation Electrocatalyst: An Online Electrochemical Mass Spectrometry Study. J. Electrochem. Soc. 2010, 157,B697-B704, DOI: 10.1149/1.3328179.

[S5]Duan, D.; Yin, X.; Wang, Q.; Liu, S.; Wang, Y. Performance evaluation of borohydride electrooxidation reaction with ternary alloy Au-Ni-Cu/C catalysts. J. Appl. Electrochem. 2018, 48 (7), 835-847, DOI: 10.1007/s10800-018-1208-0.

[S6]Datta, J.; Dutta, A.; Mukherjee, S. The Beneficial Role of the Cometals Pd and Au in the Carbon-Supported PtPdAu Catalyst Toward Promoting Ethanol Oxidation Kinetics in Alkaline Fuel Cells: Temperature Effect and Reaction Mechanism. J. Phys. Chem. C 2011, 115 (31), 15324-15334, DOI: 10.1021/jp200318m.

[S7]Merino-Jiménez, I.; Ponce de León, C.; Shah, A. A.; Walsh, F. C. Developments in direct borohydride fuel cells and remaining challenges. J. Power Sources 2012, 219, 339-357, DOI:

10.1016/j.jpowsour.2012.06.091.

[S8]Oliveira, R. C. P.; Milikić, J.; Daş, E.; Yurtcan, A. B.; Santos, D. M. F.; Šljukić, B. Platinum/polypyrrole-carbon electrocatalysts for direct borohydride-peroxide fuel cells. Appl. Catal., B 2018, 238, 454-464, DOI: 10.1016/j.apcatb.2018.06.057.

[S9]Yi, L.; Yu, B.; Yi, W.; Zhou, Y.; Ding, R.; Wang, X. Carbon-Supported Bimetallic Platinum-Iron Nanocatalysts: Application in Direct Borohydride/Hydrogen Peroxide Fuel Cell. ACS Sustain Chem Eng 2018, 6 (7), 8142-8149, DOI: 10.1021/acssuschemeng.7b04438.

[S10]Duan, D.; You, X.; Liang, J.; Liu, S.; Wang, Y. Carbon supported Cu-Pd nanoparticles as anode catalyst for direct borohydride-hydrogen peroxide fuel cells. Electrochim. Acta 2015, 176, 1126-1135, DOI: 10.1016/j.electacta.2015.07.118.

[S11]Yi, L.; Wei, W.; Zhao, C.; Tian, L.; Liu, J.; Wang, X. Enhanced activity of Au－Fe/C anodic electrocatalyst for direct borohydride-hydrogen peroxide fuel cell. J. Power Sources 2015, 285, 325-333, DOI: 10.1016/j.jpowsour.2015.03.118.

[S12] Li, S.; Wang, L.; Chu, J.; Zhu, H.; Chen, Y.; Liu, Y. Investigation of Au@Co-B nanoparticles as anode catalyst for direct borohydride fuel cells. Int. J. Hydrogen Energy 2016, 41 (20), 8583-8588, DOI: 10.1016/j.ijhydene.2016.02.128.

[S13]Olu, P.-Y.; Deschamps, F.; Caldarella, G.; Chatenet, M.; Job, N. Investigation of platinum and palladium as potential anodic catalysts for direct borohydride and ammonia borane fuel cells. J. Power Sources 2015, 297, 492-503, DOI: 10.1016/j.jpowsour.2015.08.022.